



## Research Article

# Stability Analysis of Neighborhood Tunnels with Large Section Constructed in Steeply Jointed Rock Mass

Aichen Zheng <sup>1,2</sup>, Feng Huang <sup>1,2</sup>, Zhengdong Tang<sup>1,2</sup> and Zhaoyi He<sup>1,2</sup>

<sup>1</sup>School of Civil Engineering, Chongqing Jiaotong University, Chongqing 400074, China

<sup>2</sup>State Key Laboratory of Mountain Bridge and Tunnel Engineering, Chongqing Jiaotong University, Chongqing 400074, China

Correspondence should be addressed to Aichen Zheng; zheng.aichen@163.com

Received 22 November 2019; Revised 21 February 2020; Accepted 28 April 2020; Published 19 June 2020

Academic Editor: Suzanne M. Shontz

Copyright © 2020 Aichen Zheng et al. This is an open access article distributed under the Creative Commons Attribution License, which permits unrestricted use, distribution, and reproduction in any medium, provided the original work is properly cited.

To investigate the instability of two neighborhood tunnels with large crossing section during the construction, the Tushan subway station was taken as study background, which was built in steeply jointed rock mass. Based on the excavation method called traditional double side drift, numerical simulations of four different face excavation sequences in the two neighborhood tunnels were conducted to optimize construction sequence to improve the stability during tunneling. The results show that first excavation of the right tunnel produced less deformation of the tunnels due to joints dip. The effects of rock mass discontinuities on the stability of the tunnels were studied through comparison between the real condition with joints and the assumed condition without joints. Furthermore, six initial supporting systems with different parameters were compared, and the field observations of deformations along tunnel profile show good agreement with the numerical results. Based on the numerical simulation, the length of rock anchors could be designed asymmetrically, which is more economical than the symmetrical design. The optimized thickness of shot concrete and spacing of steel sets was 35 cm and 60 cm, respectively.

## 1. Introduction

Rock mass always contains some discontinuities such as joints which are considered as a softer and weaker region than surrounding intact rock [1]. Due to sliding or detaching easily along the discontinuity plane, many unstable accidents of underground openings were reported to be closely related to joints [2–4]. The joint size is negatively correlated to tunnel stability when the other conditions are identical [5]. The stability is often significantly influenced by the size of tunnel crossing section. The subway station is a typical kind of tunnel with large crossing section, which is always more than 300 m<sup>2</sup> in Chongqing of China and has a very high risk during construction by subexcavation especially in the soft/weak ground [6]. Furthermore, neighborhood tunnels must occasionally be constructed due to either interchange or limitation of underground space. This has potential to decrease stability because of interaction between the twin tunnels. Three factors that negatively impact the stability of tunnel are (1) presence of joint, (2) large section, and (3)

small spacing. Even though all three factors rarely appear simultaneously, this work reports on the rare case when all three factors do indeed appear simultaneously. Therefore, it is necessary to develop a construction method to decrease risk and promote economic feasibility.

Stability is the most important problem in tunnel construction and is related to excavation method and support system [7]. Numerical analysis is an effective means to simulate the construction process [8]. Due to the anisotropic mechanical behavior of jointed rock mass, the discontinuum-based methods would be appropriate. The discrete element method (DEM) is the most popular for simulating the mechanical reaction during tunnel construction. For example, Vardakos et al. [9] conducted a numerical back analysis of the response of a highway tunnel during construction using DEM computer code UDEC. Funatsu et al. [10] employed the DEM commercial codes PFC2D to study the mechanism of the effects of ground supports and reinforcements on tunnel stability in a sandy ground. The discontinuous deformation analysis (DDA) is

especially applicable to solve large displacement and deformation problems. For example, Tsesarsky and Hatzor [11] studied the stability of underground openings excavated in a blocky rock mass considering the joint spacing and friction. However, due to loss efficiency of calculation and more requirement of numerical expertise, the application of discontinuum-based method usually is not possible to assist design or construction for engineers at project site. By contrast, continuum-based method is more widely used due to more efficiency and easier modeling, which mainly include finite element method (FEM) and finite difference method (FDM). For example, Satici and Ünver [12] presented assessment of tunnel portal stability at jointed rock mass at a highway in Turkey by a comparative numerical model with no jointed rock mass using FEM. Barla [13] employed FDM software FLAC to simulate the swelling phenomenon induced by the excavation of the tunnel to understand the behavior of tunnels in swelling ground. Generally, most of studies using continuum-based method are focused on some cases of intact rock mass or highway tunnel [14, 15], whereas studies such as the type in this paper are rarely reported. This paper concerns steeply jointed rock mass and supercrossing section of subway station constructed by the subexcavation method.

In this paper, two neighborhood tunnels of subway station with superlarge section at steeply jointed rock mass are taken as study example. Numerical simulations are carried out to compare different construction methods and find out the best face excavation sequence and support system parameters, which will significantly help to decrease the risk, make money, and reduce the duration of this project construction.

## 2. Engineering Background

Chongqing is a typical mountain city in the west of China with less available land, and therefore, subway system becomes one of the most important and efficient modes of transportation. There are 213 km of subway already built and with plans to construct 200 km more in the near future. Even with so many subway lines, the efficiency suffers because of the geographical conditions of mountain city, so the loop line has been constructed to deal with it. The total length of the loop line is 51 km and is made up of 33 stations. The Tushan station in this paper is one of the 13 interchange stations, which is shown in Figure 1. The subway station is located in the old pedestrian street of Nanan district in Chongqing. Some roads, building foundations, and municipal pipes will be crossed below or nearby the subway station, which means a rigid deformation will be required during tunneling.

The whole Tushan subway station is made up of two neighborhood tunnels and ten aisles for pedestrian to interchange line, as shown in Figure 2. The total length of the station is about 426 m (mile mark from DK28 + 422.648 to DK28 + 848.640). The longitudinal section profile is presented in Figure 3.

The location of DK28 + 632.848 was adopted as the study object, as shown in Figure 2, and the crossing section of

tunnels is shown in Figure 4. Each tunnel is a two-floor and island-style station with the span of 21.56 m and height of 20 m (crossing section is 375.26 m<sup>2</sup>). The site elevation is from 250 m to 281 m, and the mean cover depth of tunnel is 27.3 m. The ground layer from top to bottom is backfilled soil (0–5 m) and then either sandstone or sandy mudstone (deeper than 5 m), and there is only some fissure water inner rock mass. Based on the field geotechnical investigation, the dominant joints inner ground should be the interface between sandstone and sandy mudstone. The joint is a kind of mud structure surface with a thickness of 2–5 mm. The joint dip along tunnel axis is about 30°, and the intersection angle between them is about 14°, as shown in Figure 3. Most of joints dip in crossing section plan is about 47°, as shown in Figure 4, which indicates steeply jointed rock mass ground. The spacing between the two tunnels is 19.7 m, which means typical neighborhood tunnels.

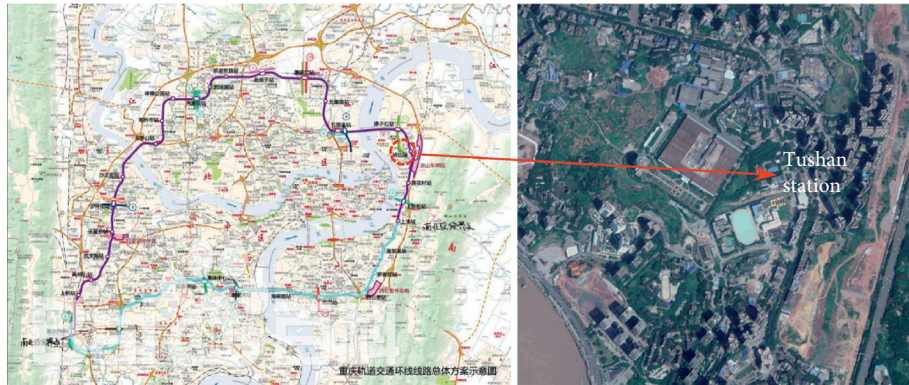
According to local experience of underground space construction in Chongqing city, the station tunnel was constructed by the subsurface excavation method of NATM (new Austria tunnel method), which could lead to a large deformation and even serious collapse during tunneling. In consequence, there is a dire need to develop the best construction method including face excavation sequence and reasonable support parameter.

## 3. Numerical Simulation Method

*3.1. Numerical Model.* Double side drift method is one of most common partial excavation methods for more effectively controlling the large deformation after tunneling, which is most popular and widely applied in subway station construction in Chongqing city, such as Linjiangmen station of line-2 [16], Daping station of line-1 [17], and Hongqihogou station of line-3 [18]. Therefore, the similar excavation method was adopted by designers.

A series of parallel numerical simulation have been performed using the commercial finite element software MIDAS/GTS. Because the axial length of tunnel is much large than the dimension of crossing section, the three-dimensional model can be reduced to a two-dimensional model [19]. According to the real dimensions, as shown in Figure 4, the numerical meshes are built, as presented in Figure 5, which include intact rock, joints, and support structure. The ground surface is free, and the other sides are constrained normally.

The ratio of in situ stress or field stresses “ $k_0$ ” is adopted as 0.55 according to the geotechnical investigation. The ground stress release ratio after excavation and before support “ $k_1$ ” is adopted as 0.6 according to the design codes of a road tunnel in China. The modeling procedures are completed by 3 steps as follows: firstly, the numerical model reaches equilibrium and produces the in situ stress field of  $k_0$ . Secondly, the following step is to excavate the tunnel face with a ground stress release ratio of  $k_1$ . Thirdly, the support system is reactivated with a remaining stress release ratio of  $1-k_1$ . The second and third steps will be iterated a few times until the whole profile of twin tunnels is formed.



(a) (b)  
 FIGURE 1: Location of the (a) tunnel area and (b) its satellite image.

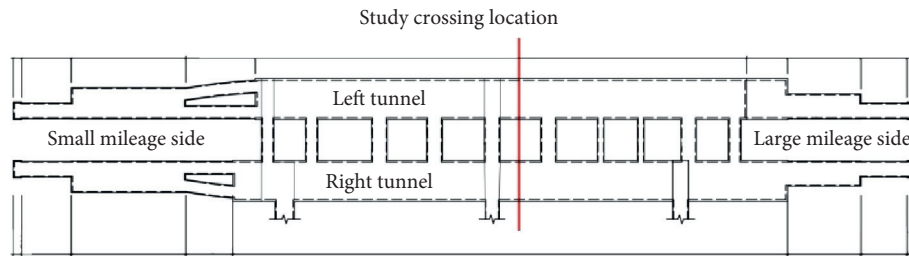


FIGURE 2: Planar graph of tunnels.

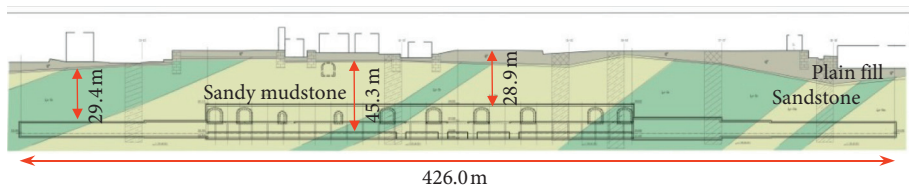


FIGURE 3: Longitude profile of tunnels.

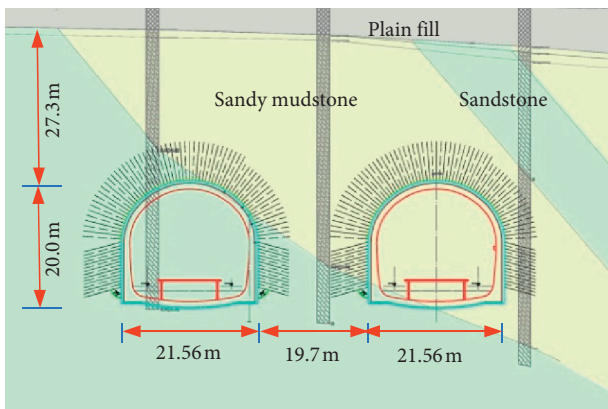


FIGURE 4: Longitude profile of tunnels.

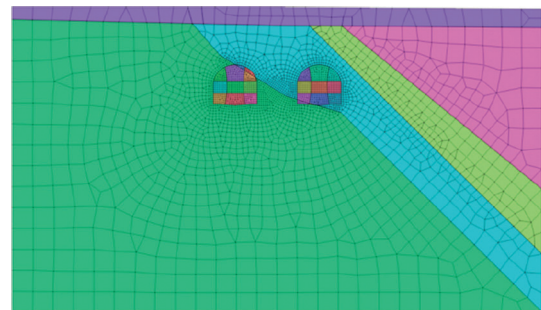


FIGURE 5: The FEM meshes for numerical simulation.

3.2. *Parameters for Calculation.* An ideal elastic-plastic constitution model based on Drucker–Prager yield criterion is employed for the solid elements of intact rock. Some

common triaxial compression tests were conducted by the machine named RMT-150C from China, as shown in Figure 6(a). The intact rock mechanical parameters are obtained, as presented in Table 1. According to the design codes of a road tunnel in China, the rock can be classified into grade IV; therefore, Poisson ratio of rock should be 0.30



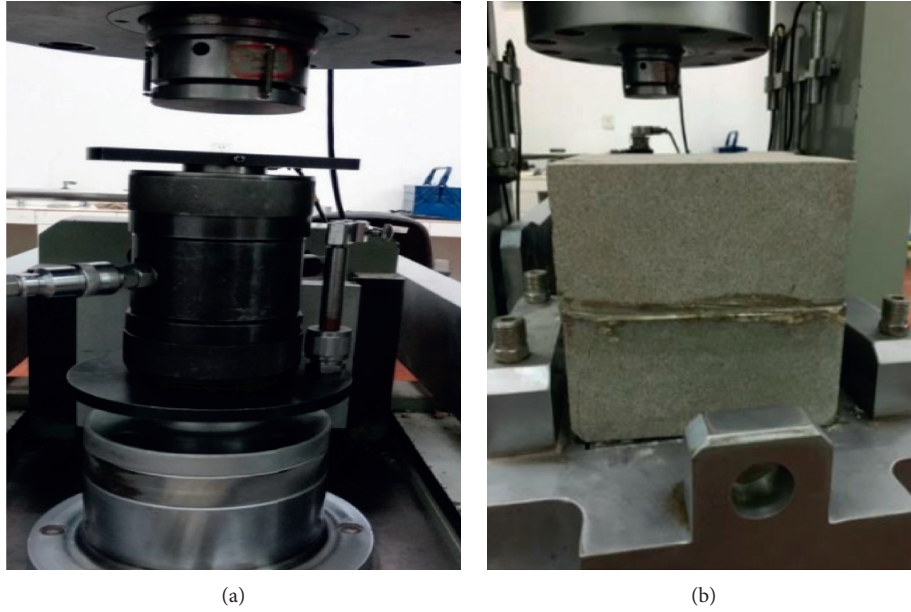


FIGURE 6: The apparatus for rock tests in laboratory: (a) common triaxial for intact rock; (b) direct shear for joint.

to 0.35, and eventually, the estimated value of 0.32 is adopted. To prove the adopted constitution model, the uniaxial compression test of model material was simulated by Midas/GTS. The relationship of axial stress and strain along the vertical direction is compared between laboratory test and numerical simulation, as shown in Figure 7, from which it can be seen that the results of numerical simulation agree well with those in the material test result. According to field investigation, the rock mass in the project site is approximately intact except the interfaces between sandstone and mudstone considered later. Therefore, the geotechnical parameters of rock mass are similar to intact rock by ignoring the size/scale effect due to little discontinuity.

The Mohr–Coulomb shear strength criterion was chosen to model interface elements of joints. It can be described as

$$\tau_{\max} = c_i + \sigma_n \tan \phi, \quad (1)$$

where  $\tau_{\max}$  is the shear strength (maximum shear stress along the interface),  $C_i$  is the cohesion,  $\sigma_n$  is the normal stress applied to the interface, and  $\phi$  is the friction angle of interface surfaces. Using the directed shear test, the shear strength can be recorded for different normal stresses also by the machine RMT-150C, as shown in Figure 6(b). The relationship between normal stress and shear strength is presented in Figure 8, and accordingly, the cohesion and friction angle are calculated to be 0.08 Mpa and  $25^\circ$ , respectively.

The normal stress  $\sigma_n$  and shear stress  $\tau_s$  are determined by

$$\begin{aligned} \sigma_n &= k_n u_n, \\ \tau_s &= \begin{cases} k_s u_s, & k_s u_s \leq \tau_{\max}, \\ \tau_{\max}, & k_s u_s > \tau_{\max}, \end{cases} \end{aligned} \quad (2)$$

where  $k_n$  and  $k_s$  are normal and shear stiffness of the interface and  $u_n$  and  $u_s$  are normal and shear displacement, respectively. Both the normal stiffness and shear stiffness of the interfaces are determined using the empirical equation [20]:

$$k_n = k_s = 10 \times \frac{K + (4/3G)}{\Delta z_{\min}}, \quad (3)$$

where  $\Delta z_{\min}$  is the smallest width of an adjoining zone in the normal direction, which is 2 mm in the established model.  $K$  and  $G$  are bulk modulus and shear modulus of the medium, respectively, which are 3.5 GPa and 1.21 GPa, respectively.

Some structure elements based on elastic model are chosen to simulate the support system, for example, beam element for shot concrete and embedded truss element for rock anchors. Steel component sets along tunnel profile are simulated by increasing elastic modulus of shot concrete based on the equivalent principle as follows [21]:

$$E_{\text{eq}} = \frac{\sqrt{[E_{\text{shot}} s + (E_{\text{steel}}/E_{\text{shot}} - 1)E_{\text{shot}} A_{\text{steel}}/d]^3}}{\sqrt{[E_{\text{shot}} s^3 + 12(E_{\text{steel}}/E_{\text{shot}} - 1)E_{\text{shot}} J_{\text{steel}}/d]}}. \quad (4)$$

The subscripts eq, shot, and steel indicate the equivalent structure, shot concrete, and steel component, respectively.  $E$  and  $A$  are the elastic modulus of substance and crossing section area,  $s$  is the thickness of shot concrete,  $d$  is the spacing distance of steel component along tunnel axis, and  $J$  is the moment of inertia of cross section. The equivalent unit weight  $\gamma$  of structure can be calculated as follows. All physical and mechanical parameters of support structure are presented in Table 2:

$$\gamma_{\text{eq}} = \gamma_{\text{shot}} + \frac{\gamma_{\text{steel}} A_{\text{steel}}}{ds}. \quad (5)$$

TABLE 1: The physical and mechanical parameters of intact rock.

Material	Unit weight (kN/m <sup>3</sup> )	Friction angle (°)	cohesion (MPa)	Elastic modulus (GPa)	Poisson ratio
Filled soil	20.5	28	0.028	0.5	0.45
Sandstone	24.9	41.5	2	3.4	0.15
Sandy mudstone	25.6	32.5	0.6	1.1	0.39

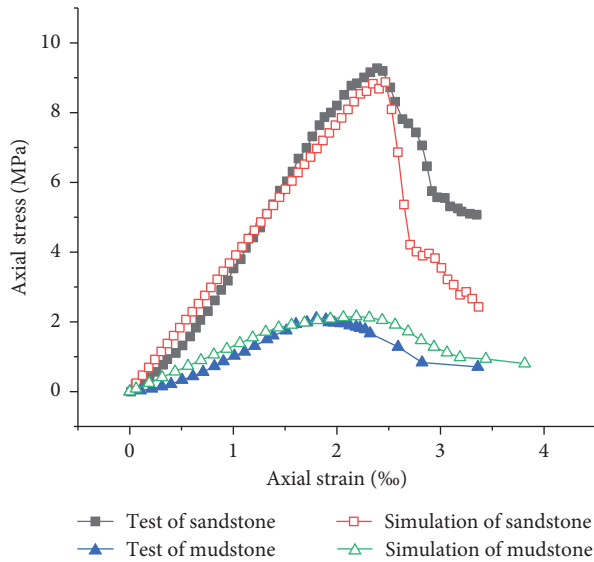


FIGURE 7: Comparison of strain-stress under uniaxial compression between test and simulation.

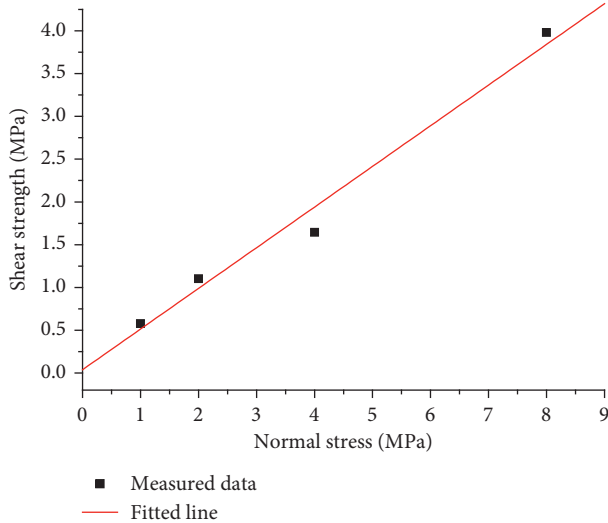


FIGURE 8: Relationship diagram of normal stress and shear stress.

3.3. *Simulation Cases.* To develop a construction method that keeps the stability of tunneling, there are three kinds of numerical cases studied in this paper.

3.3.1. *The Safer Excavation Sequences.* Four cases are studied with each having different excavation methods but same support parameters. These four cases are presented in Figure 9, where numbers with circle mean excavation

sequence. By comparative results, the better construction method of partial excavation is determined and discussed in Section 4.1. The length and spacing of rock anchor with steel of Q235 are 6.0 m and 1.0 m, respectively; the thickness of shot concrete is 0.3 m, and the spacing of steel component with type of I 25b is 0.5 m.

3.3.2. *Effect Analysis of Steep Joints.* Two cases will be studied. One case is the real situation with joints at rock mass, while the other case is the supposed situation without any joint. By comparative results, the dominant effects of joint will be discussed in Section 4.2. The excavation sequence is adopted as in Figure 9(a), and the measured points for upcoming analysis are presented in Figure 10.

3.3.3. *The More Reasonable Support System.* After determination of excavation sequences, the optimization analysis of support system was carried out for more economical cost. By comparative results of different support parameters, the optimal support system can be found out, which will be discussed in Section 4.3. Rock anchors were considered as different lengths and same spacing of 1.0 m, as shown in Table 3, where case no. 2 and case no. 4 had different lengths at right and left side walls of tunnel. Shot concrete was studied by considering different thicknesses of concrete layer and spacing of steel component, as presented in Table 4, where the results are calculated according to equations (4) and (5).

## 4. Comparison Analysis of Results

4.1. *Comparison Analysis of Excavation Sequence.* The iso-grams of vertical and horizontal deformation after all tunneling for case no. 1 are shown in Figures 11(a) and 11(b), respectively. Vertical settlement like an arch shape mainly concentrated in the zones between the two tunnels. Vertical heave mainly concentrated near tunnel invert, and the value at the right tunnel was distinctly larger than the value at the left tunnel. Horizontal deformation is mainly concentrated on the side wall especially for the intersection zones with joints. The maxima of deformation along the tunnel profile for the 4 cases with different excavation sequences are presented in Table 5. Case no. 2 is the only one where left tunneling was the first completed which results in a larger deformation than the other 3 cases. This means that first completion of right tunneling should be better than first completion of left tunneling with regard to deformation. The other 3 cases with first completion of right tunneling had deformations that resembled each other.

The isogram diagrams of rock anchor force and shot concrete stress for case no. 1 are shown in Figures 12 and 13,

TABLE 2: Parameters of support system.

Material	Unit weight (kN/m <sup>3</sup> )	Elastic modulus (GPa)	Poisson ratio	Strength (MPa)	
				Compression	Tension
Shot concrete	24.8	29.5	0.2	25	1.78
Steel component	78.5	210	0.3	235	235
Rock anchor	77	210	0.3	235	235

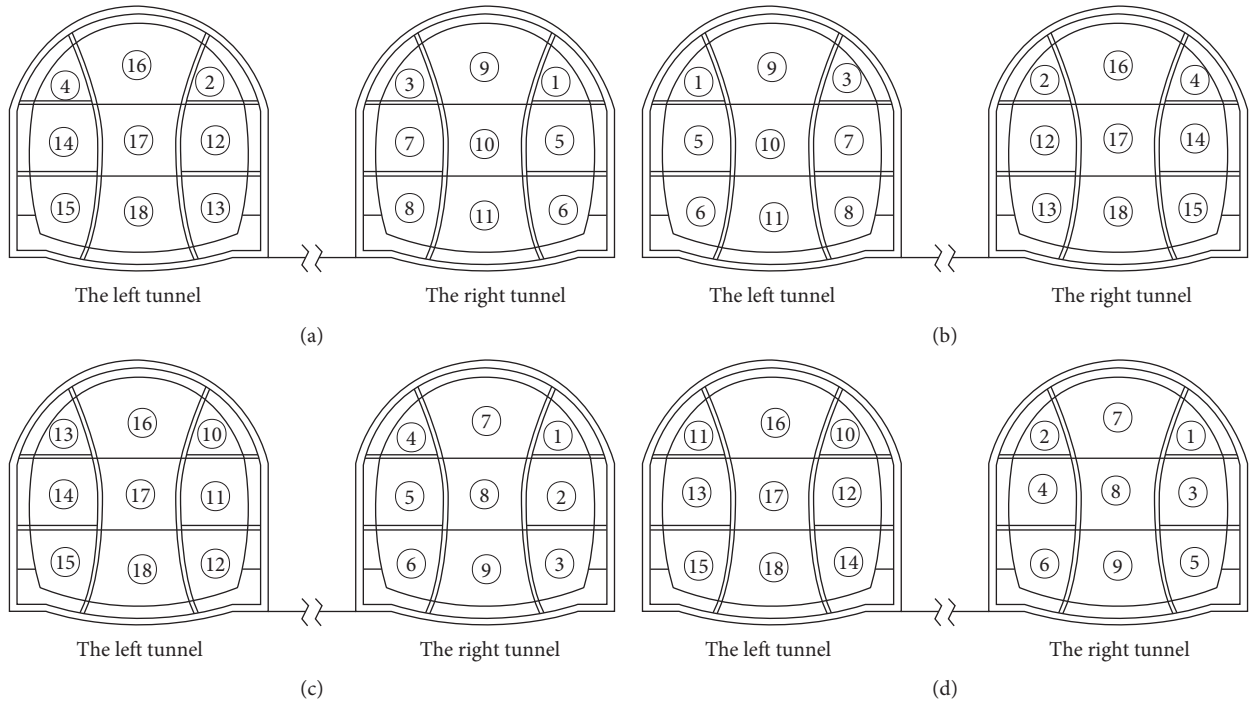


FIGURE 9: Diagrams of construction sequence for 4 cases: (a) case no. 1; (b) case no. 2; (c) case no. 3; (d) case no. 4.

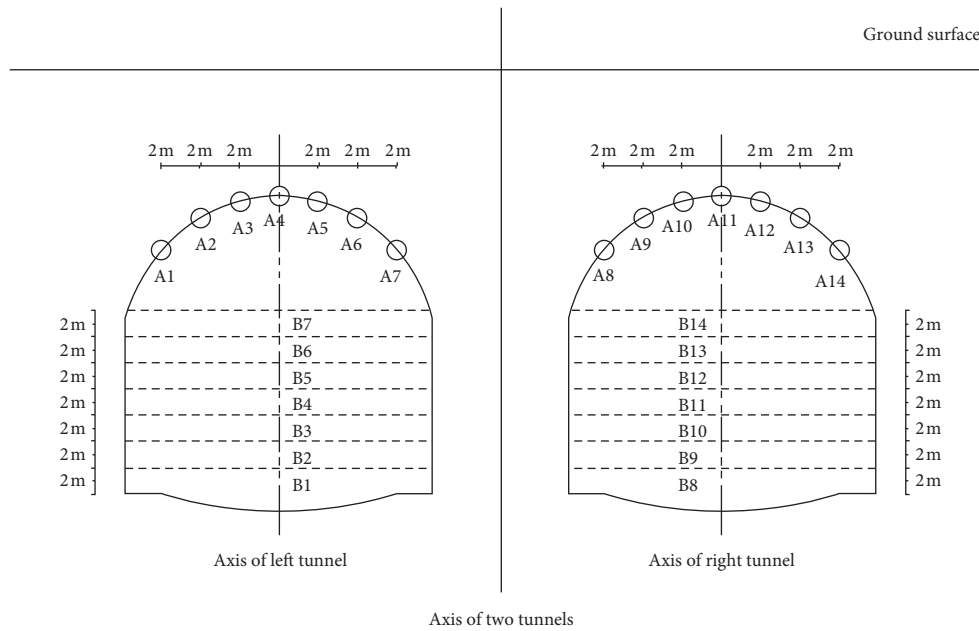


FIGURE 10: Diagram of measured points.

TABLE 3: Length of rock anchors.

Case no.	1		2		3		4		5	6
		Right wall		Left wall		Right wall		Left wall		
Length of anchors (m)	3	3		4.5	4.5	4.5		6	6	9

TABLE 4: Equivalent elastic modulus (GPa) and unity weight (kN/m<sup>3</sup>).

Spacing	Thickness				
	25 cm	30 cm	33 cm	35 cm	40 cm
40 cm	33.8/25.9	32.0/25.4	31.2/25.2	30.7/25.1	29.7/24.8
50 cm	31.6/25.3	30.2/24.9	29.5/24.8	29.2/24.7	28.4/24.5
60 cm	30.2/24.9	29.0/24.6	28.4/24.5	28.1/24.4	27.5/24.2
70 cm	29.2/24.7	28.1/24.4	27.7/24.3	27.4/24.2	26.8/24.0
80 cm	28.4/24.5	27.5/24.2	27.1/24.1	26.8/24.0	26.4/23.9

respectively. The mechanical reaction of structure generally displayed asymmetric distribution between left tunnel and right tunnel especially near the intersection zone of tunnel profile and joint. The maxima of anchor force and concrete stress for the 4 cases with different excavation sequences are presented in Table 6. Case 1 leads to a much smaller force of rock anchor than case 3 and case 4. However, it results in a slightly larger stress of shot concrete than case 3 and case 4. On the contrary, the efficiency of construction had to be considered for shortening the construction period. Case 1 had more operation face than case 3 and case 4. In conclusion, the case 1 method should be the best construction method of the 4 cases, which was also adopted in following studies.

4.2. *Comparison Analysis of Joint Effect.* The isograms of vertical and horizontal deformation after completely tunneling for the case of no joint are shown in Figures 14(a) and 14(b), respectively. For the case of no joint, the vertical deformation distributed symmetrically with maxima is located at the crown of tunnel. Compared with Figure 11, the joints make the deformation become larger in both left and right tunnels. It seems that the whole tunnel system tends to move down. Because the joints would slide to right hand, the deformation reaction influenced by joint is much more for right tunnel. The vertical deformation distribution along the arches profile of two tunnels (as points A1 to A14 in Figure 10) is compared between the 2 cases, as shown in Figure 15. The mean increment of deformation between with joint and no joint in the right tunnel is more than a factor of two greater than the left one.

The horizontal convergence along the side walls of two tunnels (as points B1 to B14 in Figure 10) is compared, as shown in Figure 16. For the case of no joint, the deformation between left tunnel and right tunnel is almost close to each other. For the case with joint, the convergence got bigger somewhere or smaller somewhere. The maxima of convergence also appeared at the right tunnel, which is roughly the same with the changing rules of vertical deformation.

The settlements along surface between the two cases after completely tunneling are compared, as shown in Figure 17.

For the case of no joint, the zone of settlement influenced by tunneling is distributed symmetrically and mainly concentrates in range between the two tunnels. The maximum locates nearby axis of model symmetry. Comparatively, the joints lead to more settlement and make maximum move to right side, which means the upcoming loading on tunnel structure will become distinctly greater and significantly more unsymmetrical.

The joints had significant influences on the mechanical reaction of rock anchors, and the maxima of anchor force are summarized in Table 7. The maxima of anchor force for the case with joint are over 2 times greater than the case with no joint. The location of maximum moves to the intersection of tunnel profile and joints.

The maxima of shot concrete stress are summarized in Table 8. It is the same as anchors reaction rule that the joints lead the increasing and moving of shot concrete stress. Fortunately, both tension stress and compression stress were much lower than the requirement of safety factor.

4.3. *Comparison Analysis of Support Optimization.* The deformation statistics of vertical settlement and horizontal convergence are presented in Figure 18. The values between case nos. 1, 2, and 3 were very close to each other, which mean anchor length would have no remarkable influence on tunnel deformation when it is less than 4.5 m. The deformations for case nos. 4, 5, and 6 are much less than the values of case nos. 1, 2, and 3. Therefore, anchor length will have notable influence on tunnel deformation when it is more than 4.5 m. The deformations between case nos. 4, 5, and 6 were close to each other, which indicate the length of anchor is unnecessary when it is more than 6.0 m. By comparing case nos. 4 and 5, the support effect is close to each other, but case 4 had anchors at left side of tunnel 1.5 m shorter than case no. 5. The maxima of anchor force with different cases of supporting system are presented in Figure 19. In consequence, the distribution of rock anchors should be designed according to case no. 4 considering both mechanical reactions and economic feasibility.

The deformation statistics of maximum vertical settlement and of horizontal convergence for different supporting parameters are shown in Figures 20 and 21, respectively. Both settlement and convergence will decrease according to the increasing thickness of shot concrete, but the slope progressively became almost constant when thickness is more than 35 cm which was adopted as the support parameter. For the same thickness of shot concrete, less spacing of steel component results in less induced deformation. However, the deformations changed inconspicuously when the spacing is less than 0.6 m which was adopted as the support parameter for economic consideration.



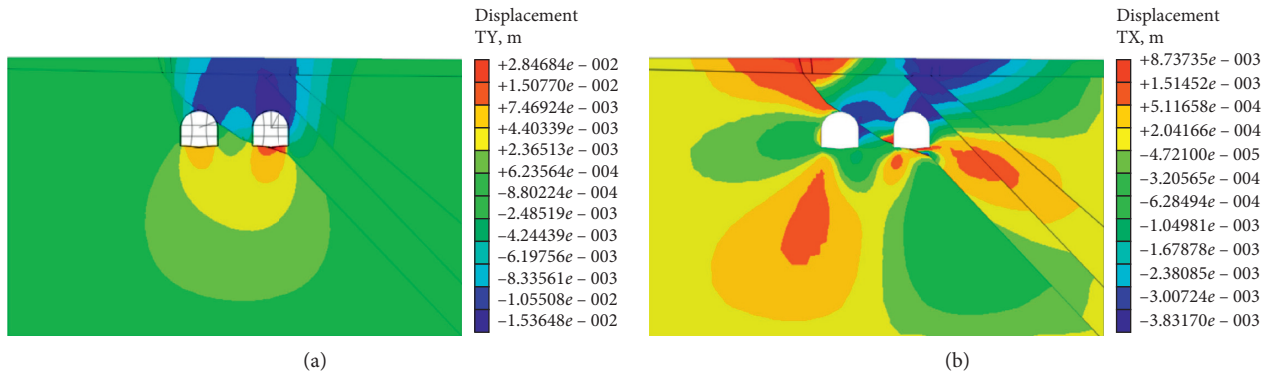


FIGURE 11: Isogram diagrams of deformation for case no. 1 after completely tunneling: (a) vertical deformation; (b) horizontal deformation.

TABLE 5: Maxima of deformation for different cases.

Case no.	Vertical direction (mm)		Horizontal direction (mm)	
	Settlement	Heave	Towards right	Towards left
1	15.36	28.46	8.74	7.63
2	15.82	28.16	10.16	6.13
3	14.90	28.05	5.22	6.34
4	15.05	28.00	8.06	6.85

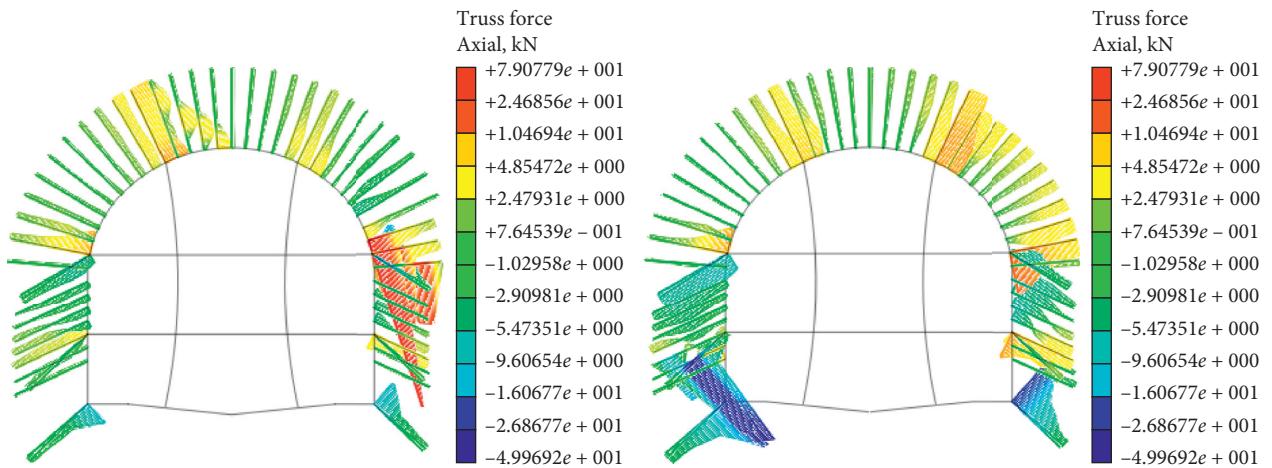


FIGURE 12: Isogram diagrams of rock anchor force for case no. 1.

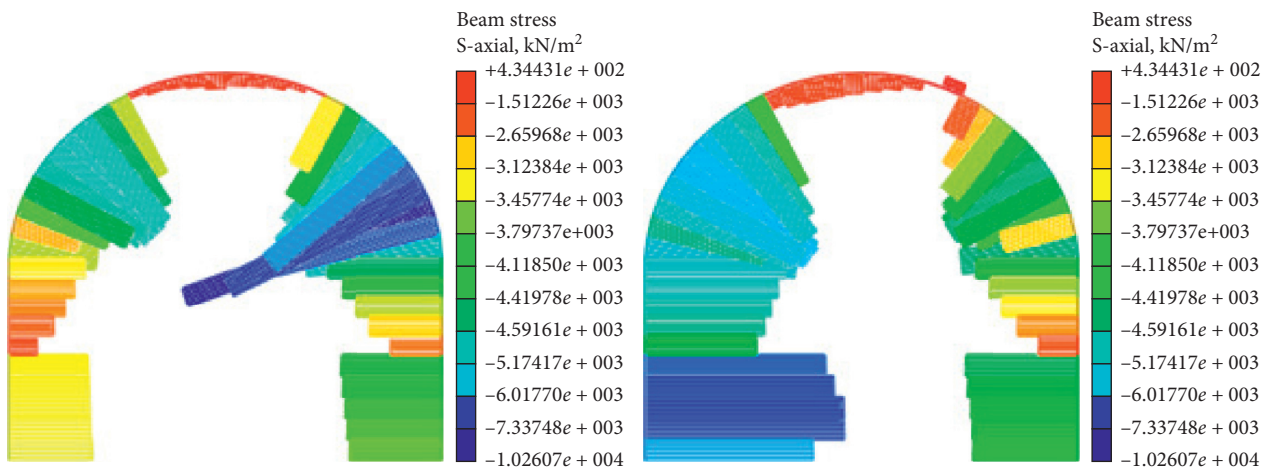


FIGURE 13: Isogram diagrams of shot concrete stress for case no. 1.



TABLE 6: Maxima of structure force or stress.

Case no.	Rock anchor force (kN)		Shot concrete stress (MPa)	
	Tension	Compressive	Compressive	Tension
1	79.08	49.97	10.26	0.44
2	58.44	41.68	9.12	0.47
3	97.53	65.75	8.12	0.38
4	98.98	50.47	8.23	0.32

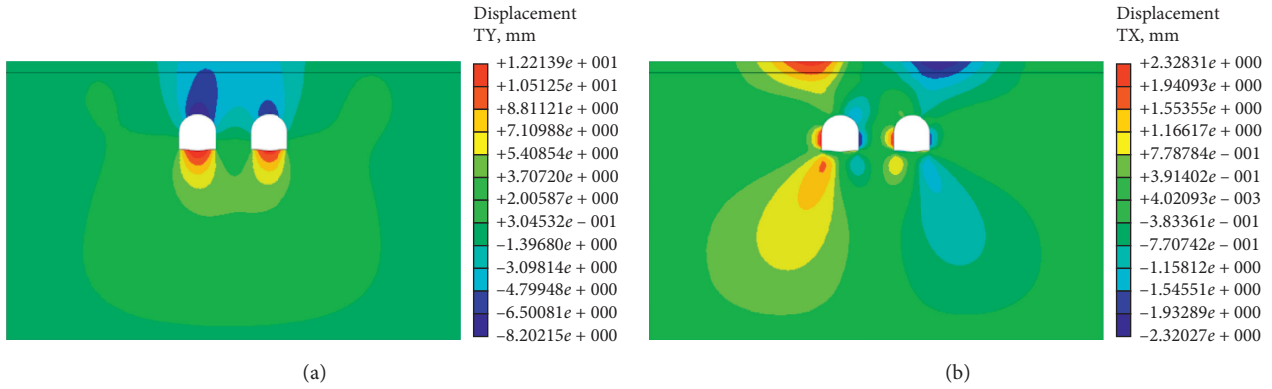


FIGURE 14: Isogram diagrams of deformation for case of no joint: (a) vertical deformation; (b) horizontal deformation.

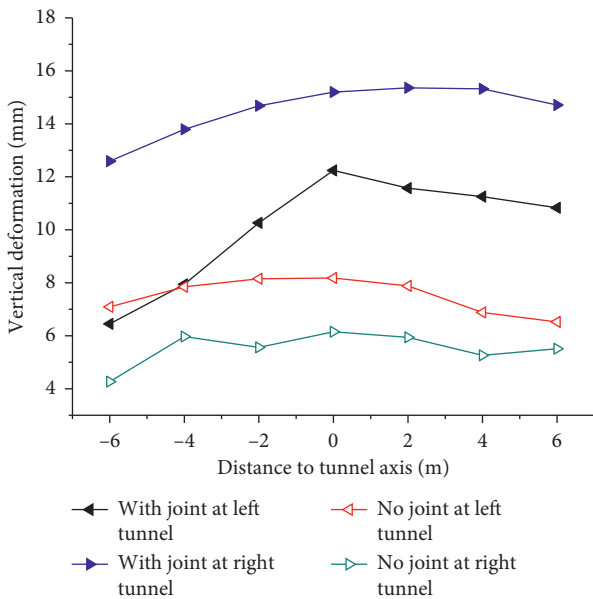


FIGURE 15: Vertical settlement curves along tunnel arch profile.

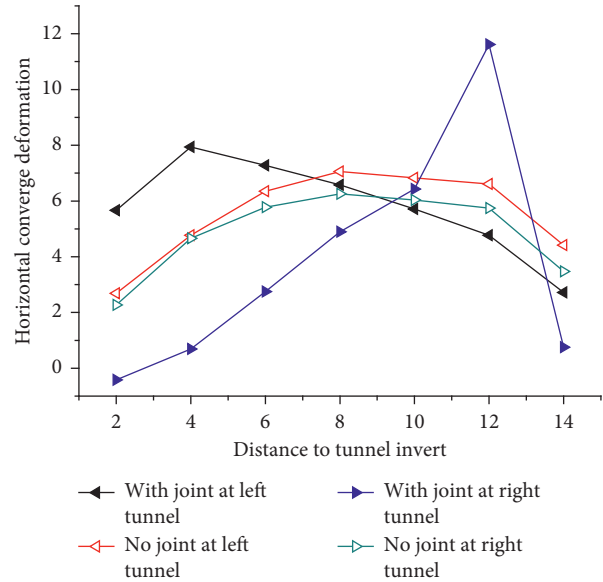


FIGURE 16: Horizontal convergence curves along tunnel side wall.

4.4. Comparison Analysis with Field Measurement. Some deformation data from field monitoring including settlement at arch roof and convergence at side wall were recorded, as shown in Figure 22. Due to the support effect of excavation face and the process of stress release, the deformation in field lasted more than one month and finally got constant as the end of curves, which means the tunnels were stable during construction. Basically, the numerical results are a bit more than the field observation. In fact, measurement devices in tunnel are always installed much later than the excavation both in space and time, which

would lead to some deformation and took place before observation. According to these studies [22, 23], 20–60% of immediate deformation could not be observed due to the delay of installation of monitoring system. By contrast, the difference for the subsidence observation on surface is much less than data inner tunnel because the monitoring work can be conducted on the ground synchronously. The subsidence data were compared between numerical simulation and field observation, as shown in Figure 23, which suggested the satisfying agreement and similar distribution rules with each other. The relative errors between numerical result and measurement data at

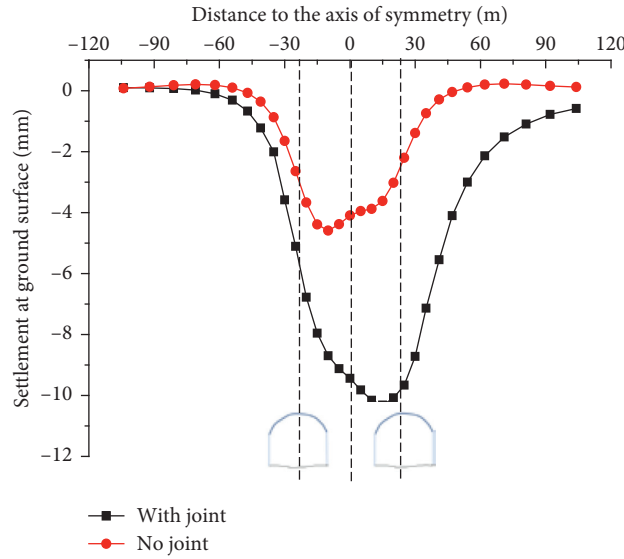


FIGURE 17: Surface settlement curves of two different cases.

TABLE 7: Maximums comparison of rock anchor.

Type of case	Maximum of tensile force			Maximum of compressive force		
	Value (kN)	Safety factor	Location near	Value (kN)	Safety factor	Location near
With joint	79.08	1.46	Left shoulder of left tunnel	-49.97	2.31	Left side wall of right tunnel
No joint	29.11	3.96	Crown of right	-15.54	7.42	Right foot of left tunnel

Safety factor is equal to the ratio between strength and force of rock anchor.

TABLE 8: Maximum comparison of shot concrete.

Types of case	Maximum of compressive stress			Maximum of tensile stress		
	Value (MPa)	Safety factor	Location near	Value (MPa)	Safety factor	Location near
With joint	-10.26	2.44	Right shoulder of left tunnel	0.44	4.05	Right shoulder of right tunnel
No joint	-4.25	5.88	Right shoulder of left tunnel	0.34	5.24	Crown of left tunnel

Safety factor is equal to the ratio between strength and stress of shot concrete.

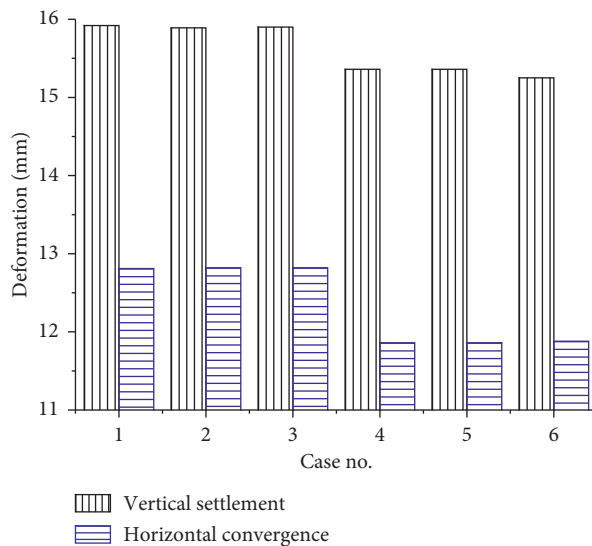


FIGURE 18: Maxima of deformation for different cases of supporting.

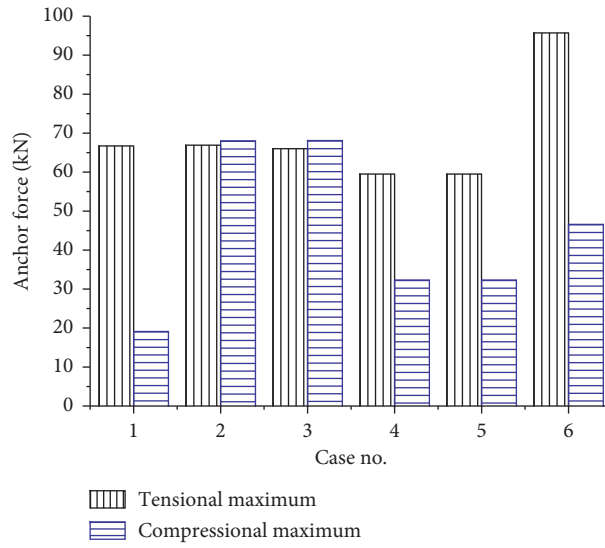


FIGURE 19: Maxima of anchor force for different cases of supporting.

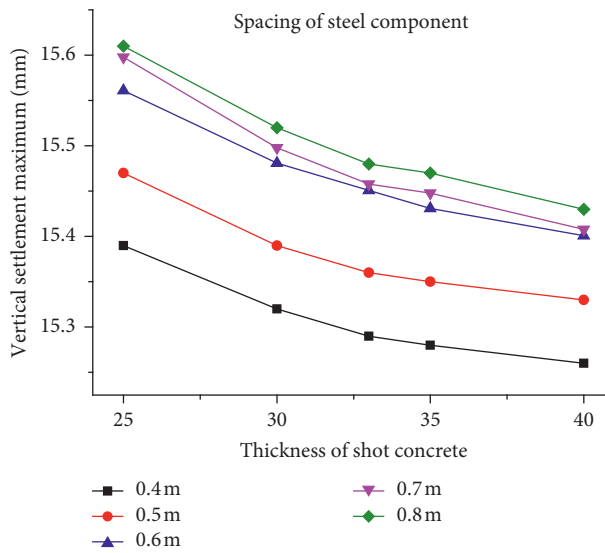


FIGURE 20: Maximum settlements changing curve with supporting parameters.

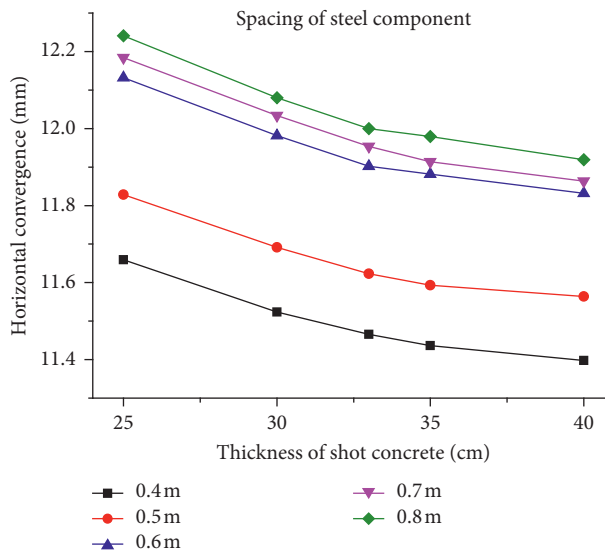


FIGURE 21: Maximum convergences changing curve with supporting parameters.

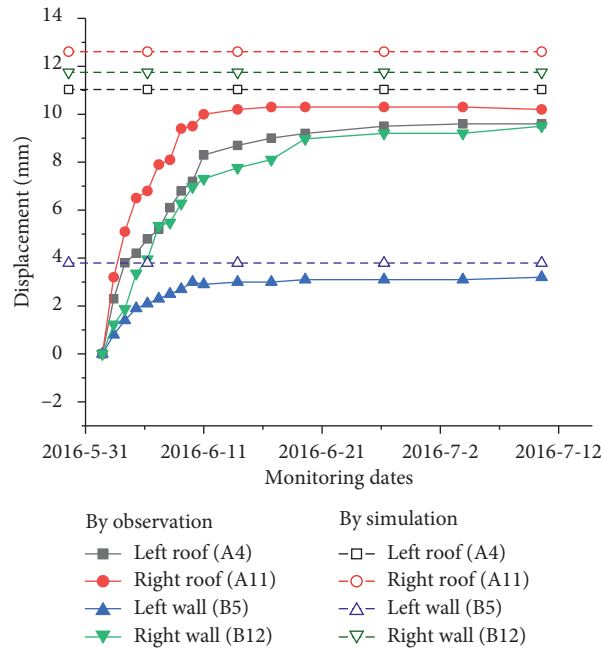


FIGURE 22: Displacements of settlement and convergence obtained from field monitoring.

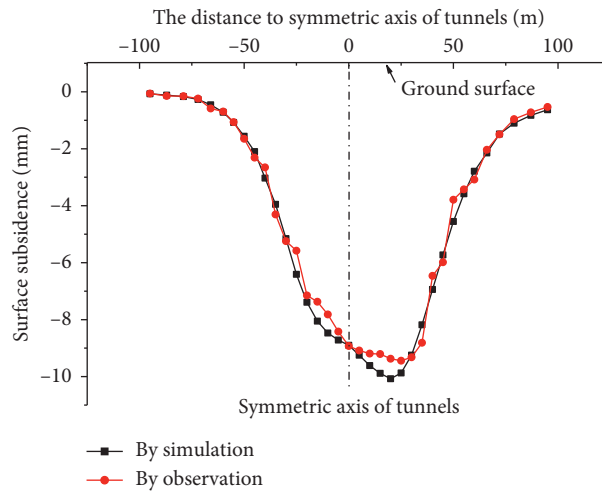


FIGURE 23: Comparison of surface subsidence between simulation and observation.

TABLE 9: Result comparison of measured points.

Measured position, number	Numerical result (mm)	Measurement data (mm)	Relative error
Left roof, point A4	11.03	9.6	14.9%
Right roof, point A11	12.61	10.3	22.4%
Left wall, point B5	3.79	3.1	22.2%
Right wall, point B12	11.75	9.5	23.7%
Maxima of surface subsidence	10.07	9.41	6.5%

The position of points is shown in Figure 10.

different measurement locations in this study are presented in Table 9, which indicates numerical simulation has an acceptable agreement with field observation. Generally, both of the deformation maxima and speed at measured points are

under the standard of stability according to Chinese road tunnel construction codes. Eventually, the underground subway station made up of many tunnels was constructed safely and finished in July 2017.



## 5. Conclusions

By taking two neighborhood tunnels of subway station with supersection at steeply jointed rock mass as an application example, some numerical simulations have been conducted for finding out the most reasonable construction method for this special underground structure. Based on these investigations, some conclusions can be drawn as follows:

- (i) The face excavation sequence like traditional double side drift was adopted. Due to the special location relations between tunnels and joints, the better excavation sequence should be first completing the right tunnel rather than the left because of less deformation of tunnel and inner force of support system.
- (ii) By adding discontinuities and keeping other details the same, the dominant effects of joint on construction stability have been proved by some concentrations of deformation and increasing inner force of structure near the intersection between tunnel profile and joint.
- (iii) The reasonable length of rock anchor should be unsymmetrically designed for saving cost and almost the same support effect. The reasonable thickness of shot concrete and spacing of steel component should be 35 cm and 60 cm, respectively.
- (iv) The deformations by field observation show good agreements with the results of numerical simulation and meet the requirements for the stability of tunnels during construction.

## Data Availability

Some or all data, models, or code generated or used during the study are available from the corresponding author on request.

## Conflicts of Interest

The authors declare that they have no conflicts of interest.

## Acknowledgments

This work was financially supported by the National Key Research and Development plan (no. 2018YFB1600200), National Natural Science Foundation of China (no. 51308574), special project of social and people's livelihood from Chongqing Science and Technology Commission (cstc2016shmszx30009), and financial plan of China Scholarship Council (no. 201608505105).

## References

- [1] F. Huang, H. Zhu, Q. Xu, and X. Cai, "The effect of weak interlayer on the failure pattern of rock mass around tunnel-scaled model tests and numerical analysis," *Tunnelling and Underground Space Technology*, vol. 35, no. 4, pp. 207–218, 2013.
- [2] G. Bruneau, D. B. Tyler, and J. Hadjigeorgiou, "Influence of faulting on a mine shaft—a case study: part I—Background and instrumentation," *International Journal of Rock Mechanics and Mining Sciences*, vol. 40, no. 1, pp. 95–111, 2003.
- [3] M. Potvin and T. Onargan, "Influence of the fault zone in shallow tunneling: a case study of Izmir Metro Tunnel," *Tunnelling and Underground Space Technology*, vol. 33, no. 1, pp. 34–45, 2013.
- [4] S. Panthee, P. K. Singh, A. Kainthola, and T. N. Singh, "Control of rock joint parameters on deformation of tunnel opening," *Journal of Rock Mechanics and Geotechnical Engineering*, vol. 8, no. 4, pp. 489–498, 2016.
- [5] P. Jia and C. A. Tang, "Numerical study on failure mechanism of tunnel in jointed rock mass," *Tunnelling and Underground Space Technology*, vol. 23, no. 5, pp. 500–507, 2008.
- [6] F. Huang, B. Liang, G. X. Wang, L. Chen, and Z. Wu, "The study and application of "interlaid rock wall" method in the subway station with shallow buried depth and large crossing section," in *Proceedings of the Tunneling and Underground Construction*, Shanghai, China, May 2014.
- [7] E. Hoek, "Big tunnels in bad rock," *Journal of Geotechnical and Geoenvironmental Engineering*, vol. 127, no. 9, pp. 726–740, 2001.
- [8] W. Zhu, S. Li, S. Li, and C. F. Chen, "Systematic numerical simulation of rock tunnel stability considering different rock conditions and construction effects," *Tunnelling and Underground Space Technology*, vol. 18, no. 5, pp. 531–536, 2003.
- [9] S. S. Vardakos, M. S. Gutierrez, and N. R. Barton, "Back-analysis of Shimizu Tunnel No. 3 by distinct element modeling," *Tunnelling and Underground Space Technology*, vol. 22, no. 4, pp. 401–413, 2007.
- [10] T. Funatsu, T. Hoshino, and H. Sawae, "Numerical analysis to better understand the mechanism of the effects of ground supports and reinforcements on the stability of tunnels using the distinct element method," *Tunnelling and Underground Space Technology*, vol. 23, no. 5, pp. 561–573, 2008.
- [11] M. Tsesarsky and Y. H. Hatzor, "Tunnel roof deflection in blocky rock masses as a function of joint spacing and friction—a parametric study using discontinuous deformation analysis (DDA)," *Tunnelling and Underground Space Technology*, vol. 21, no. 1, pp. 29–45, 2006.
- [12] Ö Satici and B. Ünver, "Assessment of tunnel portal stability at jointed rock mass: a comparative case study," *Computers and Geotechnics*, vol. 64, no. 3, pp. 72–82, 2015.
- [13] M. Barla, "Numerical simulation of the swelling behaviour around tunnels based on special triaxial tests," *Tunnelling and Underground Space Technology*, vol. 23, no. 5, pp. 508–521, 2008.
- [14] F. S. Jeng, M. C. Weng, T. H. Huang et al., "Deformational characteristics of weak sandstone and impact to tunnel deformation," *Tunnelling and Underground Space Technology*, vol. 17, no. 3, pp. 69–82, 2002.
- [15] M. Cai, "Influence of stress path on tunnel excavation response-numerical tool selection and modeling strategy," *Tunnelling and Underground Space Technology*, vol. 23, no. 6, pp. 618–628, 2008.
- [16] L. H. Huang, C. G. Cheng, S. P. Jiang et al., "Study on design and construction of main structure of light rail underground station," *Chinese Journal of Rock Mechanics and Engineering*, vol. 24, no. 10, pp. 1715–1721, 2005.
- [17] Z. B. Zhu, X. R. Liu, and Y. X. Zhang, "Study of excavation method for ultra-shallow-buried light railway station tunnels with large span," *Chinese Journal of Rock Mechanics and Engineering*, vol. 24, no. 2, pp. 290–295, 2005.

- [18] G. X. Wang, L. G. Xiao, and Y. L. Wang, "Discussion on excavation methods of shallow-covered extra-large cross-section urban tunnels," *Tunnel Construction*, vol. 29, no. 6, pp. 56–67, 2009.
- [19] G.-q. Zhang, "Rock failure with weak planes by self-locking concept," *International Journal of Rock Mechanics and Mining Sciences*, vol. 46, no. 6, pp. 974–982, 2009.
- [20] N. Barton and V. Choubey, "The shear strength of rock joints in theory and practice," *Rock Mechanics*, vol. 10, no. 1-2, pp. 1–54, 1977.
- [21] C. Carranza-Torres and M. Diederichs, "Mechanical analysis of circular liners with particular reference to composite supports. For example, liners consisting of shotcrete and steel sets," *Tunnelling and Underground Space Technology*, vol. 24, no. 5, pp. 506–532, 2009.
- [22] K. F. Bizjak and B. Petkovšek, "Displacement analysis of tunnel support in soft rock around a shallow highway tunnel at Golovec," *Engineering Geology*, vol. 75, no. 1, pp. 89–106, 2004.
- [23] M. J. Kavvadas, "Monitoring ground deformation in tunneling: current practice in transportation tunnels," *Engineering Geology*, vol. 79, no. 1-2, pp. 93–113, 2005.